Microstructural evolution in melt-quenched amorphous Se during mechanical attrition

F. Q. Guo and K. Lu
State Key Laboratory for RSA, Institute of Metal Research, Chinese Academy of Sciences, Shenyang 110015, People's Republic of China
(Received 27 October 1997)

Microstructural evolution of an as-quenched amorphous Se sample during ball milling was investigated by use of x-ray diffraction, a differential scanning calorimeter, infrared and Raman spectroscopy, as well as x-ray photoemission spectroscopy. It was found that the as-quenched amorphous Se is crystallized completely into a nanocrystalline trigonal Se phase after milling for 30 min. Further milling of the as-milled nanocrystalline trigonal Se resulted in a transformation into another amorphous Se phase, which exhibits a lower crystallization temperature and a smaller crystallization enthalpy compared to those for the as-quenched amorphous Se according to thermal analysis. Infrared and Raman spectroscopy measurements revealed that the as-milled amorphous Se is mainly composed of Se_n polymeric chains that are fundamentally different from the as-quenched amorphous Se in which the Se_8 ring structure is predominant. However, despite the phase evolution and changes in molecular structure in Se, x-ray photoemission measurements indicated that no detectable changes in electronic properties (e.g. the density of valence states, the binding energies of core levels, and the characteristic energy loss functions) were observed among different states of Se samples.
[S0163-1829(98)00417-2]

I. INTRODUCTION

In recent years, mechanical attrition (MA) has been proved to be an effective approach to induce phase transformations between metastable nonequilibrium states such as amorphous solids and nanophases. Both the amorphous-to-nanocrystalline and the nanocrystalline-to-amorphous phase transitions have been observed during MA processes.[1–11] During MA of amorphous alloys, heavy plastic deformation was introduced, resulting in a large localized permanent strain in shear band, that may be able to activate the nucleation of crystals. In an Al-based amorphous ribbon, nm-sized crystallites were observed in bending-induced shear bands.[2,9] A complete nanocrystallization was realized by ball milling of Al- and Fe-based amorphous alloys.[7–9] Meanwhile, it has been reported that in many cases MA of nanocrystalline phases may induce complete (in some alloy systems[2,5]) or partial (such as in element Si,[1,3] Ge) (Ref. 10) amorphization. The amorphization by MA is attributed to the accumulation of point and lattice defects that raises the free energy of the defective nanophase above that of the amorphous solid. However, these two processes are fundamentally opposite in direction from the thermodynamic point of view. It therefore seemed of interest to carry out an intensive study on MA-induced phase transformations between the amorphous and nanocrystalline states in a simple element system.

In the present work, we selected the as-quenched element Se to demonstrate the microstructure evolution during the MA process. It is known that Se is one of few glass-forming elements. The solid Se may have four allotropes: the amorphous phase (a-Se) and three types of crystalline structure trigonal (t-Se), α-, and β-monoclinic Se, of which t-Se is composed of Se_n polymeric chains, Se_8 rings for α- and β-Se, and a mixture of predominant Se_8 rings and partial Se_n chains for a-Se.[12,13] Every form of Se exhibits a character of a molecular material, characterized by that the groups of atoms are associated into molecules with strong internal bonding and weaker bonding between atoms on different molecules.[14] Different forms of Se have different ratios of the bonding strength, and hence different molecule vibration modes in the infrared and Raman spectra. Many related works have been done and the fundamental vibration modes of Se in various forms have been identified,[12,15,16] which enables us to employ infrared and Raman spectroscopy techniques to investigate molecular structure evolution during MA of Se. Moreover, the electron properties of the crystalline and amorphous modifications of Se have been studied intensively,[17–20] including the density of valence states, the binding energies of core levels, as well as the characterization energy loss functions. With these data the effect of MA on the electron properties of the milled Se samples can be evaluated by means of x-ray photoemission spectroscopy measurements.

II. EXPERIMENTAL

The as-quenched amorphous pure (99.999 at. %) Se specimen was prepared by melt quenching as the starting material for ball milling. The amorphous nature of the as-quenched Se was verified using x-ray diffraction (XRD). Ball milling experiments of the as-quenched a-Se were performed in a high-energy vibrating mill (Super-Misuni, Nisshin-Giken) under a flowing argon atmosphere. The milling temperature of the vial was kept at 0 °C. The ball-to-sample weight ratio is 8:1. Structural evolution was monitored using a Rigaku x-ray diffractometer (Rigaku, D/Max 2400, 12 kW) with Cu $K\alpha$ radiation and graphite monochrometer. Thermal analysis was performed on a differential scanning calorimeter (DSC-7, Perkin-Elmer) at a heating rate of 20 K/min. Characterization of the molecular structure was carried out by means of infrared (IR) and Raman spectroscopy (RS) techniques. RS measurements were performed on a Nicolet 910 FT-Raman spectrometer equipped with a Nd:YOV_4 solid laser source (the wavelength of the laser is 1064 nm). The

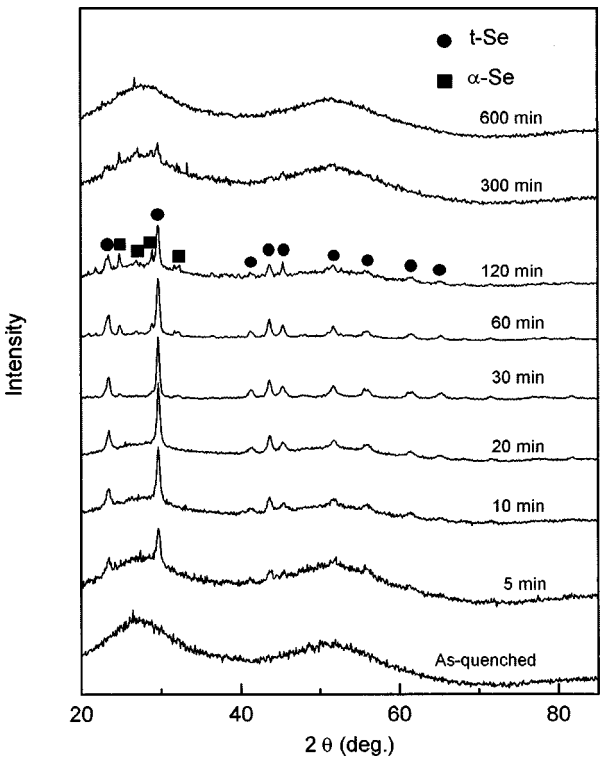

FIG. 1. XRD patterns for the as-quenched a-Se and the Se samples milled for different periods of time as indicated.

Raman spectra were recorded at a resolution of 4 cm^{-1} with 200 scans per spectrum in the range of 100–600 cm^{-1}. The laser down to the sample was defocused from a diameter of 1 to 2 mm to minimize the localized heating on the sample. The sample for Raman measurements was consolidated into disks from the milled powders. IR measurements were made using a Nicolet Magna FTIR-750 II spectrometer equipped with a diffuse reflection accessory. The IR spectra were recorded at a resolution of 8 cm^{-1} with 128 scans per spectrum in the range of 100–400 cm^{-1}. The IR samples were prepared by diluting the milled Se powders with polytene powders at a weight ratio of 1:10. The electron properties of the Se samples were determined on a LAS-3000 surface analysis system with Al $K\alpha$ radiation. The milled Se samples were consolidated into disks and then the disk surface was cleaned by ion sputtering. The cleaned specimens were put into the analyzing chamber at a pressure of 2×10^{-9} Torr. The binding energy and the zero scale of the Fermi level were calibrated by means of Cu $2p_{3/2}$ and $3p$ and Ni $3d$ levels, respectively.

III. RESULTS AND DISCUSSION

A. XRD characterization of the microstructure evolution

Figure 1 presents the XRD patterns for the as-quenched a-Se and the Se samples milled for different periods of time. One can see that the as-quenched a-Se exhibits a typical amorphous nature with two diffuse peaks in the XRD pattern. During the initial stages of milling, traces of t-Se diffraction lines appear. After milling for 10 min, t-Se diffraction lines increase obviously in their intensities at the expense of the a-Se diffuse peaks. When the milling time exceeds 30 min, only t-Se can be observed in the XRD pattern, indicating that the a-Se has crystallized completely into crystalline t-Se during milling. From the XRD line broadening, the mean grain size of the as-milled crystalline t-Se was estimated to be about 13 nm, coinciding with the TEM observations. Bright field TEM images indicated that the as-milled t-Se is composed of randomly distributed crystalline fibers, the thickness and the width of the fibers are comparable with a value of 20 nm. Dark field TEM images revealed that every of the fibers in the bright field TEM images is not a single crystal, rather a polycrystal consisting of fine equiaxial grains (about 15 nm). The corresponding electron diffraction circles showed that these nanograins have random crystallographic orientations. Their microstructure characteristics are rather similar to the crystallization products obtained thermally.[21]

TABLE I. Comparison of the crystallization temperature T_p and crystallization enthalpy ΔH for the as-quenched and as-milled a-Se samples.

	T_p (°C)	ΔH (J/g)
as-quenched	181	63
as-milled	95	44

Upon further milling of the as-milled nanocrystalline t-Se, it is noted that the XRD lines for t-Se gradually decrease, while those for α-Se appear together with the emergence of the diffuse peaks for a-Se, as shown in Fig. 1. Further milling resulted in a substantial depression in the amount of t-Se and a significant increase of the a-Se. After 600 min of milling, a fully as-milled a-Se was obtained. It should be pointed out that MA may also induce a complete amorphization of a crystalline t-Se which was thermally crystallized from the as-quenched a-Se solid.[4] A comparable XRD pattern of the a-Se was obtained as in the present case.

Despite the similarity in XRD patterns for the as-quenched and the as-milled a-Se, DSC measurements revealed marked differences between them. The as-quenched a-Se exhibits a much higher crystallization temperature (T_p) and a much larger crystallization enthalpy (ΔH) compared with the as-milled a-Se, as listed in Table I. These differences imply that these two a-Se possess different microstructures, which can also be seen in the forthcoming section.

B. RS and IR characterization of the molecular structure evolution

Figure 2(a) shows the Raman spectra for the as-quenched a-Se and the Se samples milled for different periods of time, Figs. 2(b) and 2(c) represent the amplified spectra in the range of 100–180 cm^{-1} and 350–600 cm^{-1}, respectively. Four bands were observed for the as-quenched a-Se sample: the 135 cm^{-1} band and its weak shoulder at 112 cm^{-1}, the 250 cm^{-1} band, and the 490 cm^{-1} band, of which the 250 cm^{-1} band is predominant in intensity. After milling for 0.5 min, the 112 cm^{-1} shoulder band disappeared, the 135 cm^{-1} band shifts to 141 cm^{-1} [Fig. 2(b)]. A new band at 235 cm^{-1} emerges at the expense of the 250 cm^{-1} band. For the sample milled for 5 min, the 250 cm^{-1} band can not be observed yet, the 235 cm^{-1} band increases obviously in in-

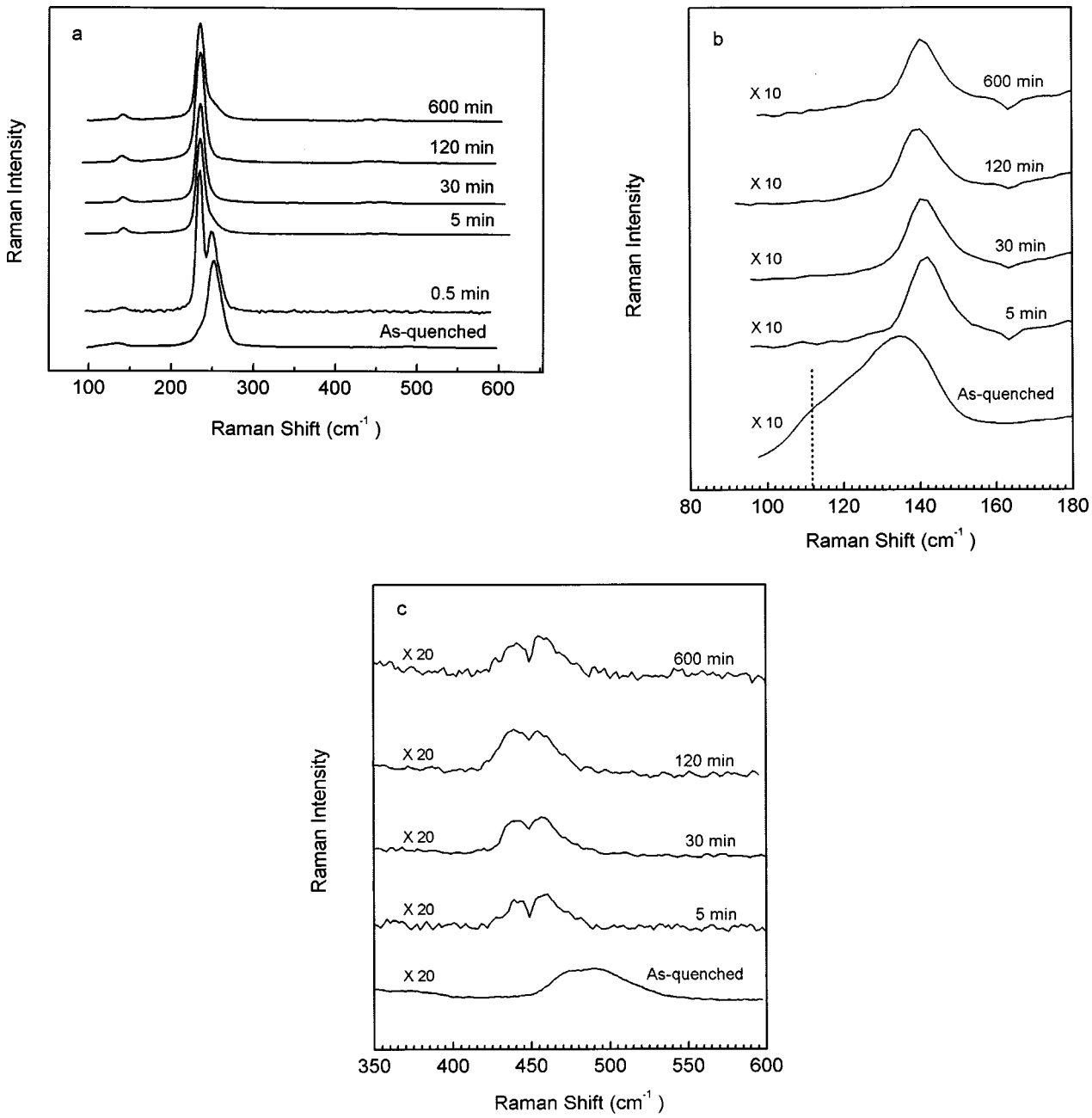

FIG. 2. (a) Raman spectra for the as-quenched a-Se and the Se samples milled for different periods of time as indicated, (b) and (c) represent the amplified spectra in the ranges of 100–180 cm^{-1} and 350–600 cm^{-1}, respectively.

tensity and becomes dominating. In addition, two new bands at 440 and 460 cm^{-1} appear whereas the 490 cm^{-1} disappeared. Further milling of the Se samples does not induce any further change in the Raman spectra.

Figure 3 gives the infrared spectra for the as-quenched a-Se and the Se samples milled for different periods of time. One can see that all the infrared spectra are divided into two parts: the 100–150 cm^{-1} band collection and the 258 cm^{-1} band with a shoulder at 230–240 cm^{-1}. Upon milling, the position of the 258 cm^{-1} band remains unchanged with its intensity decreasing substantially, while variations both in intensity and in position were observed for the bands in the range of 100–150 cm^{-1}. In the meantime, a new band at 100–104 cm^{-1} appears for all the milled Se samples while the pre-existed 119 cm^{-1} band disappeared for the Se samples milled for 5, 30, and 600 min.

As we observed from the XRD results, the milled Se samples underwent a complicated phase transformation, from the initial single phase a-Se, to a mixture of a-Se and t-Se, a single phase t-Se (30 min), a mixture of a-Se, α-Se, and t-Se, and finally a single phase a-Se (600 min) during the whole MA process. We also know that t-Se is composed of Se_n polymeric chains, Se_8 rings for α-Se and a mixture of Se_8 rings and Se_n chains for a-Se.[12] Hence for the samples with two or more phases, the analysis of the RS and IR spectra will be much more difficult because of the overlapping of the characteristic bands of Se_n chains and Se_8 rings. Here we only selected the above three single phase Se samples for a comparative study. The t-Se thermally crystallized from the as-quenched a-Se was also measured for comparison, as given in Fig. 3.

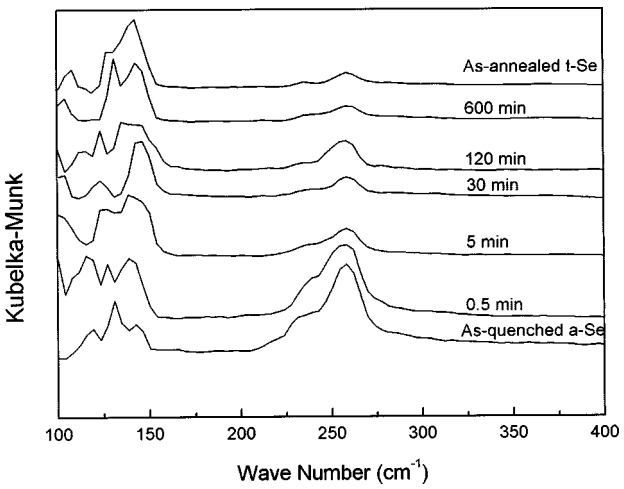

FIG. 3. Infrared spectra for the as-quenched a-Se and the Se samples milled for different periods of time as indicated.

Table II summarized the observed band positions (expressed by the vibration frequencies) and the assigned vibration modes for the four single phase Se samples. Comparing the two a-Se samples, one can see that for the as-milled a-Se a new band at 104 cm^{-1} (A_2 mode of Se_n chains) appears while the pre-existed 119 cm^{-1} band (B_2 mode of Se_8 rings) has disappeared in the Raman spectra. The A_2 mode is an infrared excited rotation mode and the B_2 mode is due to the noncentral secondary interactions. These two modes are solely associated with the interactions of atoms in neighboring molecules, and have no relation to those of the intramolecular atoms. For the as-quenched a-Se, the random arrangement of the Se molecules may result in the counteraction of the effect of the rotational vibration of A_2 mode. Similarly, it is expected that the bands related to the B_2 modes of Se_8 rings should not be confirmed. However, this expectation was not observed in the present case. It might probably be due to an incomplete disordered arrangement of the Se molecules and/or the existence of a large amount of Se_8 rings in the as-quenched a-Se (as discussed later). On the other hand, the appearance of the band related to A_2 mode of Se chains in the as-milled a-Se implies that the arrangement of Se molecules is more ordered and the amount of Se_n chains is increased relative to the as-quenched a-Se, while the disappearance of the band related to B_2 mode can only be attributed to the considerable decrease of the amount of Se_8 rings. The disappearance of the 112 cm^{-1} band related to the A_1 mode of Se_8 rings in the as-milled a-Se again confirms the same conclusion. It should be noted that after milling for 0.5 min, the Se sample is still in an ''XRD'' amorphous state, the A_2 mode of Se_n chains appears in the IR spectrum while the B_2 mode of Se_8 rings has disappeared in the RS spectrum, indicating that a short period of MA has made the molecule structure change significantly. The Se_8 rings have changed into Se_n chains upon mechanical deformation. This conclusion can also be drawn from the observed relative variations in intensity of the bands related to Se_8 rings and Se_n chains. As we known, the 250 and 235 cm^{-1} bands in the RS spectra are caused separately by the vibration of the A_1 and E modes of Se_8 rings and Se_n chains, while the 258 cm^{-1} band in the IR spectra is mainly contributed to the E mode of Se_8 rings. During ball milling, the intensities of the bands related to Se_n chains increases substantially while those related to Se_8 rings decreased obviously, indicating the occurrence of the transformation of Se_8 rings to Se_n chains.

For the two sorts of t-Se, which are composed of only Se_n chains, the observed band spectra are almost identical except that the band related to A_2 mode lies at 104 cm^{-1} for the as-milled t-Se and at 107 cm^{-1} for the as-annealed t-Se. It should be pointed out that there exists a 260 cm^{-1} band in the IR spectrum for the as-annealed t-Se, which is attributed to the A_2 and E modes of Se_n chains. This reminds us that the 258 cm^{-1} band in the as-quenched a-Se might also have a contribution from the vibration of the A_2 and E modes of Se_n chains. Meanwhile, by comparison of the IR spectra for the as-milled a-Se and the as-annealed t-Se (see Fig. 3), one can see that their bands at $\sim$260 cm^{-1} have comparable in-

TABLE II. Observed frequencies and symmetry assignment for the Se samples with different states.

as-quenched a-Se		as-milled a-Se		as-milled t-Se		as-annealed t-Se	
observed frequencies (cm^{-1})	symmetry assignment and activity	observed frequencies (cm^{-1})	symmetry assignment and activity	observed frequencies (cm^{-1})	symmetry assignment and activity	observed frequencies (cm^{-1})	symmetry assignment and activity
		104	Se_n,A_2,IR	102	A_2,IR	107	A_2,IR
112	Se_8,A_1,RS						
119	Se_8,B_2,IR						
131	Se_n,A_1-A_2 IR	132	Se_n,A_1-A_2,IR	124	Se_n,A_1-A_2,IR Se_8,B_2,IR	130	A_1-A_2,IR
135	Se_n,E,RS	141	Se_n,E,RS	141	E, RS	142	E, RS
143	Se_n,E,IR	143	Se_n,E,IR	145	E, RS	143	E, IR
		235	Se_n,A_1,E,RS	235	A_1,E,RS	233	A_1,E,RS
238	Se_n,A_1,E,IR	238	Se_n,A_1,E,IR	236	A_1,E,IR	235	A_1,E,IR
251	Se_8,A_1,E,RS						
258	Se_8,E,IR, Se_n,E,IR	259	Se_n,A_2,E,IR	259	A_2,E,IR	260	A_2,E,IR

tensities, no other bands related to Se_8 rings can be observed, indicating no Se_8 rings existing in the as-milled a-Se sample.

From the variation of the relative intensity of the bands related to different Se vibration modes, we have studied the molecule structure evolution for the milled Se samples. On the other hand, from the decrease of the band frequencies of various vibration modes, one can evaluate the effect of MA on the interactions within intramolecules and between the neighboring molecules. For simplicity we refer to intramolecular bonding as primary and intermolecular bonding as secondary. It was experimentally observed in the present work that the band of A_1 and E modes shift from 250 to 235 cm^{-1} corresponding to the transformation of Se_8 rings (in the amorphous state) to Se_n chains (in the crystalline state). This is in a good agreement with the results reported in the literature.[12] A_1 and E modes are associated with both primary and secondary interactions, particularly sensitive to the secondary interactions. If the secondary interactions are omitted and the same primary interactions are assumed, the A_1 and E modes of the chain and ring forms are very close in frequencies.[20] Actually these two forms exhibit rather similar bonding lengths and angles,[22] and so the changes in the primary bonding are very small. The observed differences in the A_1 and E frequencies can be reasonably attributed to the secondary interactions, as expressed by the secondary bonding constant K_{rR}, a term resulting from the competition of primary and secondary bonding mechanisms. For the ring form of Se, previous experimental and calculated results indicated that all the secondary interactions are very small with $K_{rR} \approx 0$, while for the chain form of t-Se, the experimental value of K_{rR} is 0.012×10^5 dyn/cm and the calculated value is 0.02×10^5 dyn/cm.[12] This implies that there exists stronger secondary interactions in the chain form of t-Se, coupled with the decreased primary interactions, and hence depressed frequencies of the related modes [A_1 and E (Ref. 12)]. It is of interest that although further milling of the as-milled t-Se led to the formation of the as-milled a-Se (where Se chains dominated), whose A_1 and E modes still lies at 235 cm^{-1}. This means that the chain form of Se in the as-milled amorphous phase exhibits a comparable secondary interactions to t-Se, and stronger secondary interactions compared to the as-quenched a-Se, indicating that the geometrical packing of the Se molecules was changed significantly by MA. In as-quenched a-Se, it can be considered that the dominated Se_8 rings and some possible Se_n chains pack in a manner with weak secondary interactions. While in the as-milled a-Se, the dominated Se_n chains arrange with much stronger secondary interactions.

By comparing the two sorts of t-Se, one can see a difference in the A_2 mode. As mentioned above, the A_2 mode is independent of all internal forces of the chains. However, as a lower frequency mode, it is more affected by the geometrical arrangement of atoms in molecules. By considering the similarity in the high frequency modes, which have little dependence on the geometrical arrangement of atoms, one can conclude that these two forms of t-Se have comparable secondary interactions. Hence the observed difference in A_2 mode frequency can be attributed to the different arrangements of atoms induced by MA, or in other words, MA might make the Se_n chains bent or distorted in the as-milled t-Se.

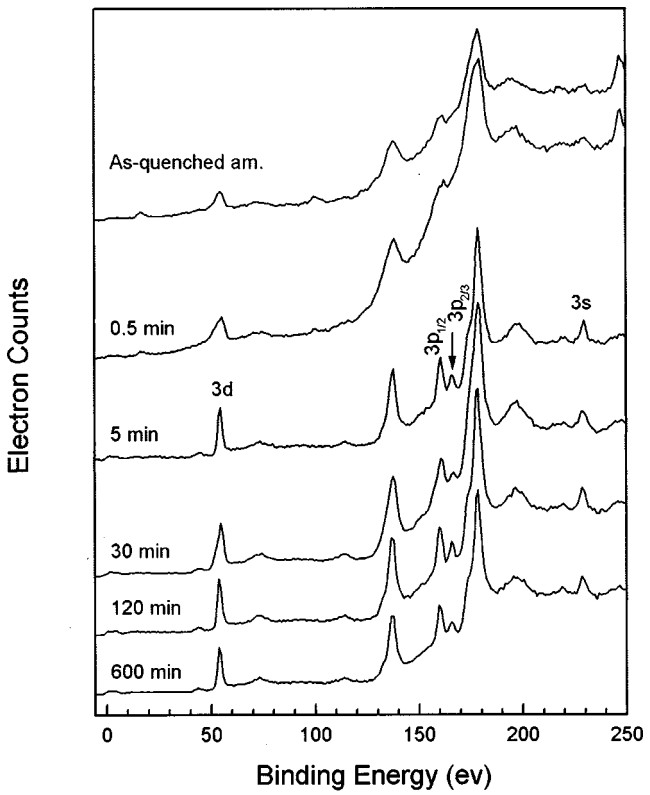

FIG. 4. XPS curves for the as-quenched a-Se and the Se samples milled for different periods of time as indicated.

As mentioned above, the as-quenched a-Se underwent a complicated structure evolution during MA. However, the IR and RS measurements did not reflect the structure changes. For example, for the Se sample milled for 120 min, which contains a α-Se phase (Se_8 rings) according to XRD, there are no bands related to Se_8 rings observed in the RS spectrum. This might mean that some alterations occurred for the internal structure of the Se_8 rings during MA. It is known that only the molecules with the polarizability varied during their vibrating are Raman active and those with the moment of dipole changed are infrared active.[23] Therefore the above observation might indicate that MA has made the Se_8 rings Raman inactive by changing the molecule symmetry. However they are still infrared active, as the band related to Se_8 rings is visible in the IR spectrum.

C. XPS characterization of the electronic properties

Figure 4 presents the XPS spectra for the as-quenched a-Se and the Se samples with different periods of milling of time. The positions of the core levels of $3d$, $3p$, and $3s$ are labeled in Fig. 4 and summarized in Table III. The binding energies of these core levels were calibrated with respect to the top of the valence band. The observed results are in good agreement with the literature data,[20,24,25] as indicated in Table III. For all the milled samples, either in the amorphous or in the crystalline states with one and more phases, the determined binding energies are quite comparable, varying relatively in narrow ranges of ± 0.2, ± 0.4, ± 0.4, and ± 0.1 eV for the $3d$, $3p_{3/2}$, $3p_{1/2}$, and $3s$ levels, respectively. Considering the limited resolution of the present XPS

TABLE III. Electron energy levels (in eV) of Se samples milled for different periods of time.

		3*d*		3*p*		3*s*	Fermi level		
Milling time (min)	Phase from XRD	level	HLW (eV)	$3p_{3/2}$	$3p_{1/2}$		*LP*	σ	4*s*
0	*a*-Se	55.0	4.2	161.4		229.9	2.0	4.9	
0.5	*a*-Se	55.2	4.7	163.0		229.9			
5	*a*- and *t*-Se	54.8	2.4	160.7	166.4	229.8	2.0	5.0	13.4
30	*t*-Se	55.0	3.2	161.3	166.9	229.7	2.2	4.9	13.5
120	*a*-*t*- and α-Se	54.8	2.6	160.9	166.8	229.8	2.3	5.1	13.4
600	*a*-Se	54.8	2.6	160.8	166.7	229.8	2.1	4.8	13.6
	20	55.1		160.7	166.5	229.6			
Values from reference	25	56.7		161.9	168.2	231.5			
	26	55.2							

(the resolution for an Alα radiation is about 1 eV), one can see that the MA process has no detectable effect on the binding energies of the milled Se samples. It is worth noting that in the as-quenched *a*-Se and the milled Se sample for 0.5 min, the energies of core levels distribute more broadly with respect to the other Se samples with a longer milling time, as can be seen in Table III, which can be attributed to the more disordered structure, and/or the charge effect induced by the lack of electron counts on the surface of semiconductor materials such as Se.[26] The charge effect was found to yield a much larger observed binding energy than in its tabulated value (here in the present experiment, an increase of 37 eV was observed in the binding energy). Moreover, the charge effect can also cause broadening of the distribution of the binding energies.[26]

It is known that there are six electrons in the valence band of Se. Two electrons per atom fill the deepest-lying *s*-like levels with a lowest energy state. The remaining four electrons fill the *p* orbitals: two of them form lone-pair bands (namely the *LP* band), while the other two spin with electrons on the nearest neighboring atoms form bands (σ band). The electrons participating in bands are expected to lie in a lower energy state than the lone-pair electrons since they are repelled by the empty antibonding states. It is hence expected that the densities of states of Se should consist of three main peaks.[27] Figure 5 shows the densities of states including 4*s* and 4*p* levels for the Se samples milled for different times. As expected, the valence bands of Se exhibit three main peaks for all the Se samples except the as-quenched *a*-Se. In the as-quenched *a*-Se, the lowest peak can not be identified due to the weak detected signals. For other Se samples, the lowest peak, centered at $\sim$13.5 eV referred to as the center in the HLW of the peak, is well separated from the upper peaks which partially overlap. The observed valence bands are also summarized in Table III. One can see that the energy states of the valence electrons for all the Se samples are comparable (within a narrow variation of symbol $\pm$0.2 eV), this is well agreeing with the literature data. The $\sim$13.5 eV peak is associated with the Se *s* bands, its $\sim$7.5 eV width implies a significant bonding of *s* bands. The $\sim$5 eV peak is associated with the σ bands, and the $\sim$2 eV peak with the *LP* orbitals. The similarity in the energy states of the valence electrons (4*s*, *LP*, and σ electrons) indicates that MA has no detectable effect on the energy states of the valence electrons.

Shevchik *et al.*[20] have studied the density of states of *a*-Se and *t*-Se by means of x-ray and far-UV photoemission techniques. They found that a triplet structure appears for the *LP* band of *t*-Se while the *LP* band of *a*-Se is only slightly asymmetric. A larger difference occurs in the σ band. The σ peak in the *a*-Se lies at 3.5 eV with a weak shoulder at $\sim$5.5 eV, while in the *t*-Se it lies at 5.5 eV with a minor peak at $\sim$3.5 eV. Zhang *et al.*[28] observed a triplet structure for the 4*s* band of Se in both amorphous and crystalline samples. The present experimental results exhibit an overall agreement with the reported literature on the structure of the valence bands. However, the splitting of the valence bands was not observed in our samples. This might be associated with the introduction of defects during the MA process and the limited resolution of the present XPS.

Figure 6 presents the characteristic energy loss spectra following the 3*d* level for the Se samples milled for different periods of time. For all the curves, the peak at zero binding energy corresponds to electrons that have escaped the sample without undergoing inelastic collisions. The resolution of the

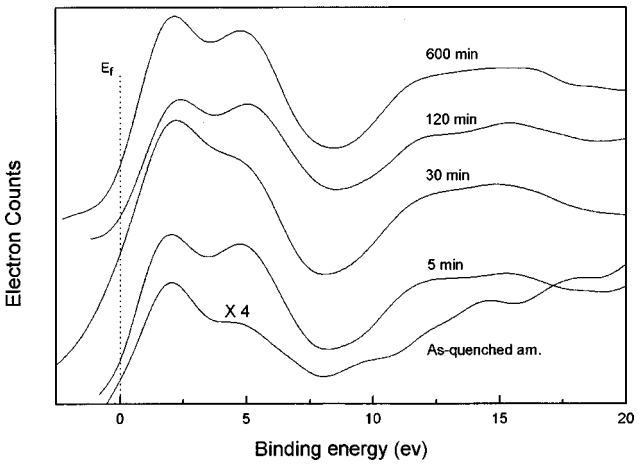

FIG. 5. Density of states including 4*s* and 4*p* levels for the as-quenched *a*-Se and the Se samples milled for different periods of time as indicated.

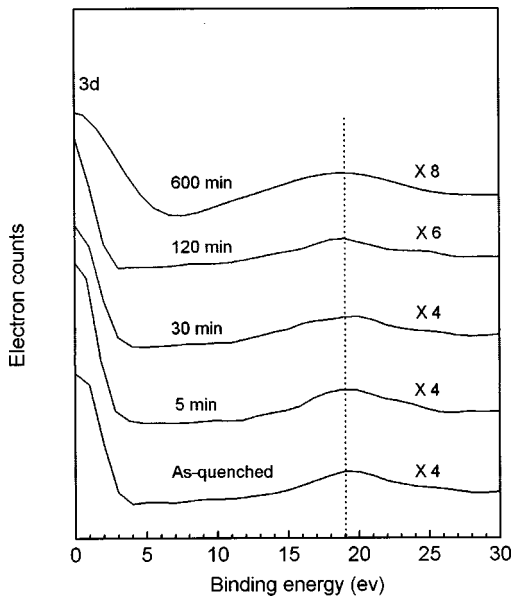

FIG. 6. Characteristic energy loss spectra for the as-quenched a-Se and the Se samples milled for different periods of time as indicated.

loss curves is given by essentially the widths of these primary peaks, and the primary peaks were aligned to fall at the same position on the abscissa axis. The loss energy was measured with respect to the center of these primary peaks. The maxima in the loss curves represent the characteristic loss energies, which occur at $\sim$19 eV for the as-quenched a-Se and all the milled Se samples, as shown in Fig. 6. It indicates no detectable effect of MA observed on the characteristic loss energies of the Se samples. However, the absence of any sharp structure in the loss peaks reveals that secondary electrons can add no structure to the deduced densities of states.

IV. CONCLUSIONS

The present work demonstrated that the MA can realize a complete transformation from an as-quenched a-Se into a nanocrystalline t-Se. Further milling induced a complete amorphization of the as-milled nanocrystalline Se. It was found that the as-milled a-Se exhibits a lower crystallization temperature and a smaller crystallization enthalpy compared to those of the as-quenched a-Se. IR and RS measurements on the molecule structure evolution of Se during the MA process revealed that the as-milled a-Se is mainly composed of Se_n chains, while Se_8 rings are predominant in the as-quenched a-Se. This means that a molecule structure transformation from Se_8 rings into Se_n chains occurred during the MA process of the as-quenched a-Se. Nevertheless, comparable electronic properties were determined for all the Se samples at different stages during the MA process, including the density of states, the binding energies of core levels, as well as the characteristic energy loss functions. In general, the MA can induce phase transformations (from amorphous to crystalline and from crystalline to amorphous) and a molecule structure evolution (from ring to chain), but has no detectable effect on the electronic properties for the pure element Se sample.

ACKNOWLEDGMENTS

We are grateful to the valuable discussions with Professor Z. H. Xu from Beijing University, and Professor W. H. Wang from the Institute of Metal Research (CAS). The financial support from the Chinese Academy of Sciences and National Science Foundation of China (Grant No. 59625101) is acknowledged.

[1] E. Gaffet, F. Faudot, and M. Harmelin, Mater. Sci. Eng., A **149**, 85 (1991).
[2] G. F. Zhou and H. Bakker, Phys. Rev. B **49**, 12 507 (1994).
[3] T. D. Shen, C. C. Koch, T. L. McCormick, R. J. Nemanich, J. Y. Huang, and J. G. Huang, J. Mater. Res. **10**, 139 (1995).
[4] G. J. Fan, F. Q. Guo, M. X. Quan, Z. Q. Hu, and K. Lu, Phys. Rev. B **55**, 11 010 (1997).
[5] J. S. C. Jang and C. C. Koch, J. Mater. Res. **5**, 498 (1990).
[6] H. Chen, Y. He, G. J. Shiflet, and S. J. Poon, Nature (London) **367**, 541 (1994).
[7] M. L. Trudeau, R. Schulz, D. Dussault, and A. Van Neste, Phys. Rev. Lett. **64**, 99 (1990).
[8] F. Q. Guo and K. Lu, Nanostruct. Mater. **7**, 509 (1996).
[9] Y. He, G. J. Shiflet, and S. J. Poon, Acta Metall. Mater. **43**, 83 (1995).
[10] E. Gaffet, Mater. Sci. Eng., A **136**, 161 (1991).
[11] F. Q. Guo and K. Lu, Philos. Mag. Lett. **77**, 181 (1998).
[12] G. Lucovsky, A. Mooradian, W. Taylor, G. B. Wright, and R. C. Keezer, Solid State Commun. **5**, 113 (1967).
[13] R. Kaplow, T. A. Rowe, and B. L. Averback, Phys. Rev. **168**, 1068 (1968).
[14] G. S. Pawley and S. J. Cyvin, J. Chem. Phys. **52**, 4073 (1970).
[15] G. Lucovsky, R. C. Keezer, and E. Burstein, Solid State Commun. **5**, 493 (1967).
[16] T. Nakayama and A. Odajima, J. Phys. Soc. Jpn. **33**, 12 (1972).
[17] J. Stuke, J. Non-Cryst. Solids **4**, 1 (1970).
[18] J. Stuke, in *The Physics of Selenium and Tellurium*, edited by W. C. Cooper (Pergamon, Oxford, England, 1969), P. 3.
[19] D. Adler, Crit. Rev. Solid State Sci. **2**, 317 (1971).
[20] N. J. Shevchik, M. Cardona, and J. Tejeda, Phys. Rev. B **8**, 2833 (1973).
[21] H. Y. Zhang, Z. Q. Hu, and K. Lu, Nanostruct. Mater. **5**, 41 (1995).
[22] P. Unger and Cherin, in *Physics of Selenium and Tellurium* (Ref. 18), p. 223.
[23] H. Q. Zhuang, in *Infrared Spectroscopy* (Chemical Industry Press of China, 1984), p. 31.
[24] J. A. Bearden and A. F. Burr, Rev. Mod. Phys. **39**, 125 (1967).
[25] D. Briggs and M. P. Seach, in *Practical Surface Analysis* (Wiley, New York, 1990), Vol. 1.
[26] J. S. Brinen, J. Electron Spectrosc. Relat. Phenom. **5**, 377 (1974).
[27] S. Tutihasi and I. Chen, Phys. Rev. **158**, 623 (1967).
[28] H. Y. Zhang, Ph.D. dissertation, Institute of Metal Research, Chinese Academy of Sciences, 1995.